Autonomous stochastic resonance driven by colored noise

Shrabani Mondal,[1] Joydip Das,[1] Bidhan Chandra Bag,[1,*] and Fabio Marchesoni[2,3]
[1]*Department of Chemistry, Visva-Bharati, Santiniketan 731 235, India*
[2]*Dipartimento di Fisica, Università di Camerino, I-62032 Camerino, Italy*
[3]*Center for Phononics and Thermal Energy Science, School of Physics Science and Engineering, Tongji University, Shanghai 200092, People's Republic of China*

(Received 29 April 2018; published 17 July 2018)

A one-dimensional linear autonomous system coupled to a generic stationary nonequilibrium fluctuating bath can exhibit resonant response when its damped oscillation period matches some characteristic bath's relaxation time. This condition justifies invoking the stochastic resonance paradigm, even if it can be achieved more easily by tuning the system to the bath and not vice versa, as is usually the case. The simple nature of the mechanism numerically investigated here suggests a number of interesting applications for instance in the context of (1) energy harvesting from random ambient vibrations, (2) activated barrier crossing through a saddle point, or (3) an unstable limit cycle.

DOI: 10.1103/PhysRevE.98.012120

I. INTRODUCTION

Stochastic resonance (SR) is a well-established paradigm in many fields of natural sciences from nanothechnology to climatology and biology [1–5]. In a broad sense, it denotes the nonmonotonic dependence of the output signal, or some function of it (like moments and signal-to-noise ratios), on the intensity of noise(s) acting on the system. This definition applies quite generally to the diverse mechanisms invoked to explain the otherwise nonuniversal SR phenomenon.

Initially, SR was proposed as a cooperative effect of noise and periodic forcing acting upon a Brownian particle confined by a bistable potential. In this context, increasing the noise correlation time was observed to degrade the SR signal [6] almost monotonically [7]. Later the SR notion was generalized to encompass *autonomous* nonlinear systems [8–10], so that external periodic drives were no longer a required ingredient. Recently two more remarkable SR mechanisms have been observed. Burada *et al.* [11], pointed out that, contrary to previous studies, in higher dimensional setups SR manifests itself even in the presence of purely entropic barriers associated with spatial constrictions. Ghosh *et al.* [12] further extended this result to demonstrate SR as a mere geometric effect.

Despite several attempts to the contrary [13], SR is currently regarded as an eminently *nonlinear* phenomenon. It is true that periodically forced harmonic oscillators subjected to a multiplicative noise do exhibit SR, in both the overdamped [14] and underdamped [15] regimes. However, as anticipated in Ref. [16], multiplicative noise generates an effective barrier that opposes the particle diffusion inside the well, so that the resulting dynamics is effectively nonlinear.

As reiterated by most authors [1], SR is not a resonance in the dynamical sense: Its magnitude cannot be maximized by simply tuning the driving frequency to some system's natural frequency at constant noise level; the periodic component of the system's response can be optimized only by tuning the noise strength.

In this paper we show that an autonomous SR mechanism can occur also in an underdamped harmonic oscillator driven by an exponentially time-correlated noise. In Sec. II we show that the output of the system attains a maximum as the damped oscillator's period matches the noise correlation time. Such a manifestation of SR carries a closer resemblance to standard dynamical resonance, a similarity corroborated by its disappearance in the overdamped regime, when autonomous oscillations are suppressed. Despite its simplicity, the model analyzed here lends itself to a number of interesting applications. In particular, it can be easily extended to model microelectromechanical systems (MEMS) for energy harvesting from random environments (Sec. III A), to calculate the activation rates through barrier saddle points (Sec. III B), and to describe barrier crossing processes through unstable limiting cycles (Sec. III C). In the concluding remarks of Sec. IV we mention the possibility of generalizing our approach to nonlinear devices or different nonequilibrium noise sources.

II. THE MODEL

Let us consider a Brownian particle of unit mass trapped in a one-dimensional harmonic potential, $U(q) = \omega_0^2 q^2/2$, of angular frequency ω_0. Its motion obeys the Langevin equation (LE)

$$\ddot{q} = -U'(q) - \gamma\dot{q} + \eta(t), \tag{1}$$

where the last two terms on the right-hand side model a minimal coupling between the particle and a stationary nonequilibrium environment. Such a coupling consists of a viscous force with damping constant γ and a stationary time-correlated Gaussian noise with zero mean value, $\langle\eta(t)\rangle = 0$, and autocorrelation function (a.c.f.) $S_{\eta\eta}(t) := \langle\eta(t)\eta(0)\rangle = (D/\tau)e^{-|t|/\tau}$. For the sake of generality, we assume that the noise intensity, D, is

*bidhanchandra.bag@visva-bharati.ac.in

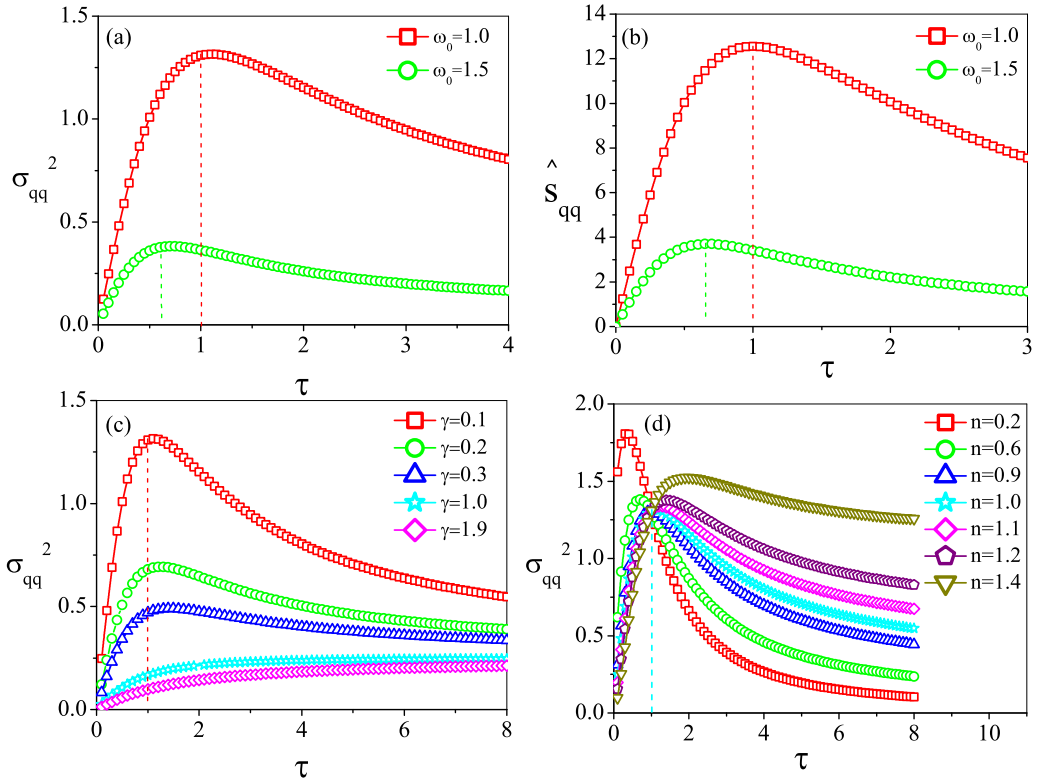

FIG. 1. Autonomous SR characterization: (a) $q(t)$ variance, σ^2_{qq} and (b) power spectral density at resonance, $\hat{S}_{qq}(\omega_d)$, (b) plotted vs τ for $\gamma = 0.1$, $n = 1$ and two values of ω_0. For a comparison we plotted σ^2_{qq} vs τ also for (c) different γ, $n = 1$ and two ω_0, and (d) different n, $\omega_0 = 1$ and $\gamma = 0.1$. The remaining parameters of Eq. (3) are $c_0 = 0.25$ and $\tau_0 = 1$. Vertical dashed lines represent the predicted optimal value, τ_c (see text).

some function of the correlation time, $D(\tau)$, so that, contrary to the standard parametrization [7], the limit $\tau \to 0$ does not necessarily correspond to an equilibrium thermal noise. Here and in the following primes and overdots are shorthand for d/dq and d/dt, respectively.

The Ornstein-Uhlenbeck process $\eta(t)$ can be easily rewritten in terms of a zero-mean valued, delta-correlated Gaussian noise $\xi(t)$: $\dot{\eta} = -\eta/\tau + \sqrt{D}\,\xi(t)/\tau$, with $S_{\xi\xi(t)} := \langle \xi(t)\xi(0)\rangle = 2\delta(t)$. Regarding $\xi(t)$ and $q(t)$, respectively, as the input and output signals, the corresponding system's square transfer function, $H^2_{q\xi}$, can be calculated as the linear mapping of the Fourier transform of the input a.c.f., $\hat{S}_{\xi\xi}(\omega) := \mathrm{FT}\{S_{\xi\xi}(t)\} = 2$, to the Fourier transform of the output a.c.f., $\hat{S}_{qq}(\omega) := \mathrm{FT}\{S_{qq}(t)\}$, with $S_{qq}(t) := \langle q(t)q(0)\rangle$:

$$H^2_{q\xi} = H^2_{q\eta} H^2_{\eta\xi} = \frac{1}{\left(\omega_0^2 - \omega^2\right)^2 + \omega^2\gamma^2} \frac{D}{1+\omega^2\tau^2}. \qquad (2)$$

The two factors in the rightmost term of the above equation are the square transfer function, respectively, between the white and the colored noise, $H^2_{\eta\xi}(\omega) := \hat{S}_{\eta\eta}(\omega)/\hat{S}_{\xi\xi}(\omega)$, and between $\eta(t)$ and $q(t)$, $H^2_{q\eta}(\omega) := \hat{S}_{qq}(\omega)/\hat{S}_{\eta\eta}(\omega)$.

The response of the damped stochastic oscillator of Eq. (1) has a maximum in correspondence with a peak, if any, of $H^2_{q\xi}$. On assuming for the time being that $H^2_{\eta\xi}$ decays more slowly than $H^2_{q\eta}$, which is the case for $\gamma\tau \ll 1$, we locate the dynamical resonance of $q(t)$ in the vicinity of the maximum of $H^2_{q\eta}$, that is for $\omega \simeq \omega_d$, with $\omega_d = \omega_0\sqrt{1-(\gamma/2\omega_0)^2}$ (for details see Appendix A). Of course, this condition holds only for moderate damping, $\gamma < \sqrt{2}\omega_0$. The resonance amplitude, $H^2_{q\xi}(\omega_d)$, is thus approximately factorized as $H^2_{q\eta}(\omega_d)[D/(1+\omega_d^2\tau^2)]$, with $H^2_{q\eta}(\omega_d) = 1/[\gamma^2(\omega_d^2+\gamma^2/16)]$.

However, the amplitude $H^2_{q\xi}(\omega_d)$ clearly depends on the correlation time and, therefore, on our choice of D as a function of τ. A quite general choice for $D(\tau)$ is

$$D(\tau) = c_0(\tau/\tau_0)^n, \qquad (3)$$

where c_0 is a heat-bath coupling constant and τ_0 an appropriate reference timescale. Thus the response of $q(t)$ is optimal when $H^2_{q\xi}(\omega_d)$ as a function of τ is maximum, that is, for $\tau = \tau_c$, with

$$\tau_c = \sqrt{\frac{n}{2-n}}\frac{1}{\omega_d}. \qquad (4)$$

Here τ_c is defined only for $0 < n < 2$ and, therefore, certainly not in the regime of constant D, $n = 0$, investigated in Refs. [6,7].

The optimal condition of Eq. (4) describes the situation when the power spectral density of the ambient fluctuations, $S_{\eta\eta}(\omega) = 2D(\tau)/(1+\omega^2\tau^2)$, is the largest at the dynamical resonance frequency, ω_d: This ensures an optimal energy transfer from the environment to the oscillator.

Numerical results

We numerically simulated the LE (1) [17] for different values of the dynamical parameters, ω_0 and γ, and of the

noise parameters, τ and n. In Fig. 1 we plot our numerical data for the oscillator variance, $\sigma^2_{qq} := S_{qq}(0) = \langle q^2 \rangle$ (for the analytical expression of it see Appendix A), and the peak value of its power spectral density, $\hat{S}_{qq}(\omega_d)$. We notice immediately that at relatively low damping the positions of the maxima of σ^2_{qq} [Fig. 1(a)] and $\hat{S}_{qq}(\omega_d)$ [Fig. 1(b)] versus τ agree quite closely with the analytical estimate, $\tau \simeq \tau_c$, of Eq. (4). Such a coincidence was expected due to the fact that, for the value of γ adopted in Figs. 1(a) and 1(b), the half-width of $H^2_{q\eta}(\omega)$ at $\omega \simeq \omega_d$ is quite narrow, $\Delta\omega_d = (\omega_d/2\omega_0)\gamma$.

The resonance phenomenon emerging from Fig. 1 can be regarded as an instance of autonomous SR in its own right. Indeed, in contrast with the current literature [1], it signals the matching between an intrinsic deterministic timescale of the system and a correlation time of the ambient fluctuations.

We discuss now in more detail the dependence of this new SR on the model parameters.

(1) ω_d *dependence:* Both σ^2_{qq} and $\hat{S}_{qq}(\omega_d)$ decrease monotonically with increasing the frequency of the dynamical resonance, ω_d; consistently with Eq. (4), the optimal correlation time, τ_c, shifts to lower values, as is apparent in Figs. 1(a) and 1(b).

(2) n *dependence:* From our derivation of τ_c, it is apparent that the SR peak, $\hat{S}_{qq}(\omega_d)$, depends on the exponent n introduced in Eq. (3). This parameter characterizes the microscopic dynamics of the fluctuating bath coupled to the oscillator and is, therefore, hardly tunable. Nevertheless, it is interesting to notice that the SR mechanism investigated here is predicted to be the weakest for $n^{\min} = 2\omega_d^2\tau_0^2/(1+\omega_d^2\tau_0^2)$. This effect is illustrated in Fig. 1(d), where the lowest SR peak occurs indeed for $n \simeq n^{\min}$ and is centered around $\tau \simeq \tau_0$, as expected from Eq. (4). For simplicity, in the following we adopted $n = 1$, i.e., constant η variance.

(3) γ *dependence:* In Fig. 1(c) we plotted σ^2_{qq} versus τ for different values of the damping constant. On increasing γ the SR peak is gradually suppressed until it totally disappears in the overdamped regime. This property is consistent with our interpretation of the SR mechanism at work here. Indeed, for $\gamma > \sqrt{2}\omega_0$ the square transfer function $H^2_{q\eta}(\omega)$ exhibits resonant behavior.

On a closer inspection, one notices that increasing γ also makes the SR peak of σ^2_{qq} in Fig. 1(c) shift to higher τ values faster than predicted by Eq. (4). The shift itself is no surprise: indeed, being ω_d is a decreasing function of γ, our analytical expression for τ_c increases with increasing γ. Corrections to the approximate factorization argument introduced to estimate τ_c are negligible as long as $\gamma\tau \ll 1$, as in Figs. 1(a) and 1(b). However, the width of the resonance peak of $H^2_{q\eta}$ in Eq. (2) is proportional to γ and, thus, cannot be neglected in the intermediate damping regime. As a consequence, all spectral frequencies in the interval $|\omega - \omega_d| \leqslant \Delta\omega_d$ contribute to the variance of $q(t)$. This suggests replacing τ_c of Eq. (4) with its average taken over such a frequency interval: $\bar{\tau}_c = \tau_c/[1 - (\Delta\omega_d/\omega_d)^2] = \tau_c/[1 - (\gamma/2\omega_0)^2]$. With this correction, the SR condition of Eq. (4) works well over the entire range $0 < \gamma < \sqrt{2}$.

III. APPLICATIONS

Autonomous SR results from the interplay of two basic memory effects: inertia (mechanical memory) and noise autocorrelation (environmental memory). Moreover, we restricted our analysis to a linear model, which allowed a fully analytical solution of the model equations (see Appendix A). For these reasons it is no surprise that the results of Sec. II can apply, to a different degree of approximation, to many different physical systems.

A. Harvesting mechanical energy from ambient fluctuations

The highly idealized model considered sofar could be easily implemented by means of especially designed electronic or optical devices to serve as analog simulators of the LE (1) [1]. A more interesting application is suggested by the microelectromechanical system (MEMS) prototyped by the authors of Ref. [18] with the ultimate goal of harvesting mechanical energy from ambient fluctuations and/or vibrations. They realized an autonomous piezoelectric oscillator with tunable mechanical parameters. The electrical output of such device at constant noise level turned out to be optimal for an appropriate bistable (i.e., nonlinear) configuration of its components. We suppose here to operate the very same MEMS in its (far from optimal) linear configuration, but, at the same time, to control the correlation time of the random noise source coupled to it. In our notation, the device is governed by the equations [18]

$$\begin{aligned} \ddot{q} &= -\omega_0^2 q - \gamma\dot{q} - k_v V + \eta(t), \\ \dot{V} &= k_c\dot{q} - V/\tau_p, \end{aligned} \tag{5}$$

where k_v and k_c are piezoelectric parameters [19], $V(t)$ is the voltage output, and $\tau_p = RC$ is the characteristic time of a signal pickup RC circuit. Following Ref. [18], we further assume constant noise variance $\langle \eta^2 \rangle = D(\tau)/\tau = c_0$, i.e., $n = 1$ in Eq. (3). Our analysis of the model LE (1) can be easily extended to the linear system of Eqs. (5). The Fourier transforms (FTs) of Eqs. (5) read

$$\hat{q}\left[-\omega^2 + \omega_0^2 + i\omega\gamma + \frac{i\omega k_c k_v}{i\omega\frac{1}{\tau_p}}\right] = \hat{\eta}, \tag{6}$$

$$\hat{V} = \frac{i\omega k_c \hat{x}}{i\omega + \frac{1}{\tau_p}}, \tag{7}$$

hence the FT of the voltage auto-correlation function,

$$C_V(\omega) = \frac{\omega^2(\omega^2 + \frac{1}{\tau_p^2})k_c^2 \hat{S}_{\eta\eta}(\omega)}{\left[(\omega_0^2 - \omega^2)(\omega^2 + \frac{1}{\tau_p^2}) + k_c k_v \omega^2\right]^2 + \omega^2\left[\gamma(\omega^2 + \frac{1}{\tau_p}) + \frac{k_c k_v}{\tau_p}\right]^2}, \tag{8}$$

the spectral function $S_{\eta\eta}(\omega)$ being given in Sec. II. Upon integrating $C_V(\omega)$ with respect to ω, we obtain the voltage stationary variance,

$$\langle V^2 \rangle_s = \frac{2D}{\pi}\int_0^{+\infty} \frac{\omega^2(\omega^2 + \frac{1}{\tau_p^2})k_c^2}{1+\omega^2\tau^2} \frac{d\omega}{\left[(\omega_0^2 - \omega^2)(\omega^2 + \frac{1}{\tau_p^2}) + k_c k_v \omega^2\right]^2 + \omega^2\left[\gamma(\omega^2 + \frac{1}{\tau_p}) + \frac{k_c k_v}{\tau_p}\right]^2}. \tag{9}$$

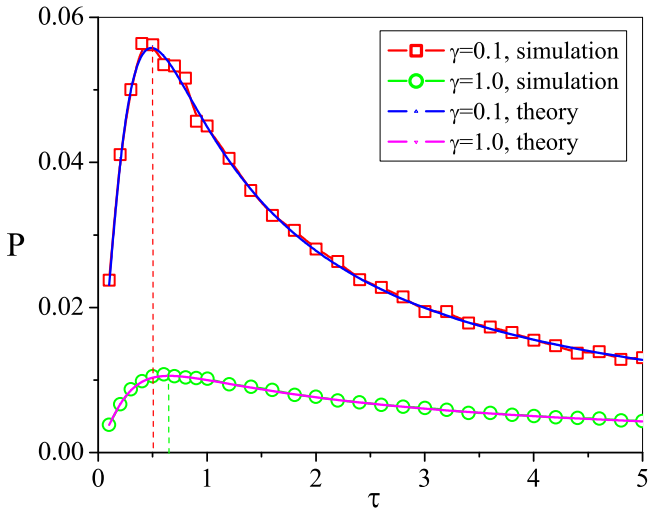

FIG. 2. Output power, P, vs τ, for the MEMS of Ref. [18] operated at resonance in the linear regime: simulation data points (symbols) from Eqs. (5) vs analytical predictions (curves) for different γ. Vertical dashed lines are the predicted optimal values, τ_c. The remaining model parameters are $c_0 = 0.25, n = 1, \tau_0 = 1, k_c = k_v = 1.0, \tau_p = 2, R = 1$, and $\omega_0 = 2$, all expressed in arbitrary units.

Using the above equation the resonant output power of the MEMS is measured by the quantity

$$P = \frac{\langle V^2 \rangle_s}{R_L} = \frac{2D}{\pi}\left(\frac{k_c}{\tau_p}\right)^2 \int_0^\infty \frac{1+\omega^2\tau_p^2}{1+\omega^2\tau^2}\,\frac{\omega^2 d\omega}{h(\omega)}, \qquad (10)$$

where $h_0 = [(\omega_0^2 - \omega^2)(\omega^2 + 1/\tau_p^2) + k_c k_v \omega^2]^2 + \omega^2[\gamma(\omega^2 + 1/\tau_p) + k_c k_v/\tau_p]^2$. The output power, P, is plotted in Fig. 2 as a function of the noise correlation time for the low and high damping constant in the operating regime, $\omega_0\tau_p \gg 1$, of Ref. [18]. The analytical curves fit well the data points obtained by numerically integrating Eqs. (5). Both numerical curves exhibit prominent SR peaks centered around an optimal value, $\tau_c \simeq 1/\sqrt{\omega_0^2 + k_c k_v}$. We expect this SR behavior to be soon experimentally validated also by measurement on real MEMSs.

B. Rate of barrier crossing through a saddle point

As a further application, we now explore the effects of autonomous SR in the barrier crossing problem [20]. To this purpose in Eq. (1) we used a bistable potential, $U(q) = aq^4 - bq^2$, with symmetric minima (wells) at $q_\pm = \pm\sqrt{b/2a}$, separated by an energy barrier, $\Delta U = b^2/4a$, centered at the origin. Following Refs. [21,22], we have calculated the approximate barrier crossing rate,

$$k = \frac{\omega_\pm}{2\pi}\left[\frac{\kappa\phi_s}{s(\kappa\phi_s + \gamma)}\right]^{\frac{1}{2}} \exp\left[-\frac{\gamma\Delta U}{s\phi_s}\right], \qquad (11)$$

where $\kappa = \lambda_0/(\phi_s + \epsilon\psi_s)$, $\epsilon = -(\gamma + \sqrt{\gamma^2 + 4\omega_b^2})/2s$ $s = 1 + \gamma\psi_s/\phi_s$, and $\lambda_0 = -\omega_b^2/\epsilon s$. Here $\omega_b^2 = 2b$ and $\omega_\pm^2 = 4b$ denote the absolute values of $U''(q)$, respectively, at the barrier top and the well bottoms. The quantities ϕ_s and ψ_s are the stationary values of the auxiliary variables $\phi(t) = \omega_\pm^2\sigma_{q\dot{q}}^2 + \gamma\sigma_{\dot{q}\dot{q}}^2 + \frac{1}{2}\dot{\sigma}_{\dot{q}\dot{q}}^2$ and $\psi(t) = \omega_\pm^2\sigma_{qq}^2 + \gamma\sigma_{q\dot{q}}^2 + \dot{\sigma}_{q\dot{q}}^2 - \sigma_{\dot{q}\dot{q}}^2$, where the cross-correlations $\sigma_{i,j}^2$, with $i, j = q, \dot{q}$, have been calculated around the potential minima in Gaussian approximation (for details see Appendix B).

To check the validity of our estimate for k, we have numerically simulated the barrier crossing process for a time-correlated noise, $\eta(t)$, of strength also given by Eq. (3) with $n = 1$. In Fig. 3(a), the crossing rate is plotted versus the noise correlation time. The agreement between the analytical prediction of Eq. (11) and the numerical data is quite good. The nonmonotonic behavior of $k(\tau)$ is a clear-cut signature of autonomous SR. This conclusion is supported by the plots of Fig. 3(b), which show how the effective activation energy of the process is itself a nonmonotonic function of τ. Another property peculiar to autonomous SR is apparent in Fig. 3(a). As already noticed in Fig. 1(c), the SR peak of the curve $k(\tau)$ gets suppressed at relatively high damping. Condition for the rate constant to exhibit autonomous SR, is that the motion around the potential minima executes damped oscillations. Of course, for D constant, i.e., $n = 0$ in Eq. (3), one recovers the well-known Kramers' problem in the presence of colored noise [23,24].

We stress that the SR mechanism for barrier crossing illustrated in Fig. 3(a) is quite distinct from the well-known resonant activation over a fluctuating barrier [25] in that here resonance does not involve a fluctuating barrier [26], but rather noise activation in the potential wells.

C. Rate of barrier crossing through an unstable limit cycle

As a final example of autonomous SR we investigated a variation of the van der Pol equation [27] with colored additive noise, $\eta(t)$, of strength $D(\tau)$,

$$\ddot{q} = -\omega_0^2 q - \gamma\dot{q}(1 - \mu^2\dot{q}^2) + \eta(t), \qquad (12)$$

recently employed to model escape processes through an unstable limit cycle [28]. In sharp contrast with Kramers' mechanism [3], these processes do not rely on noise activation from a stable state to some unstable saddle point in the (free) energy landscape, but rather on the dynamical switch between a stable attractor and an unstable limit cycle. Escape processes of this class have been advocated in biology, chemistry, and physics to interpret a variety of phenomena far from equilibrium [28,29]. In the noiseless limit, $\eta(t) \equiv 0$, Eq. (12) has a fixed point, $q = \dot{q} = 0$ independent of μ. Note that for $\mu = 0$ Eq. (12) is the same as Eq. (1) with $U(q) = \omega_0^2 q^2/2$. However, in the presence of a negative damping term, $\mu > 0$, the fixed point is enclosed by an unstable limit cycle. The interplay of the potential and the negative damping thus produces a dynamical barrier, which the Brownian particle of coordinate $q(t)$ must overcome to escape from the attractor. Having set to zero the particle's energy at the fixed point, the escape activation energy is the sum of the kinetic and potential energy of the particle on the limit cycle (a key difference with saddle-point escape). Moreover, the particle can leave the attractor through any point of the manifold in the phase space $(q, \dot{q})$ associated with the unstable limit cycle.

After rescaling Eq. (12) for $\mu = 1$, we numerically computed the escape rate $k(\tau)$ as the reciprocal of the first diffusion time of the Brownian particle in phase space between the origin, (0,0), and any point $(q, \pm 2)$. An approximate rate could

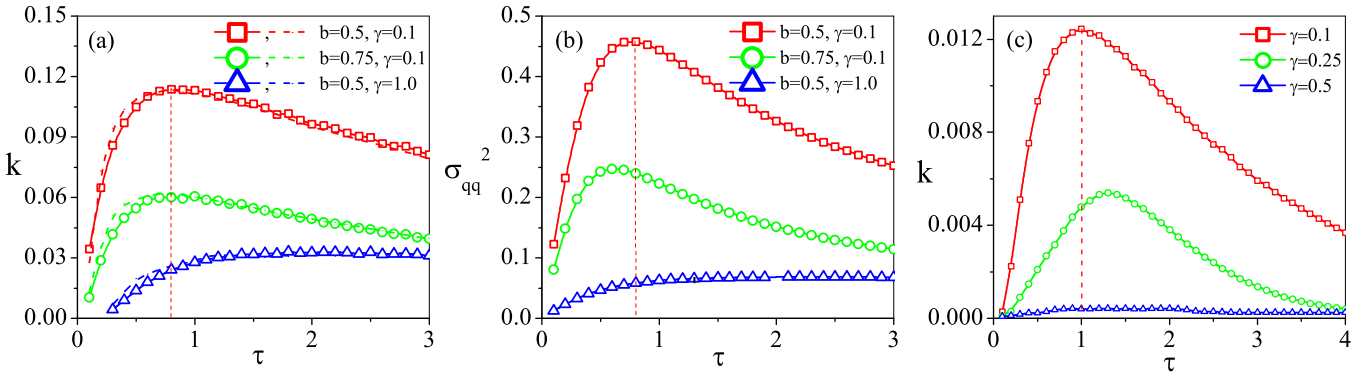

FIG. 3. Saddle-point crossing rates: (a) $k(\tau)$, in a bistable potential, $U(q)$: numerical data (symbols) vs analytical predictions, Eq. (11) (curves); (b) σ^2_{qq} vs τ in a harmonic well with the same frequency, $\omega_b^2 = 2b$, as the bistable wells of $U(q)$. The parameter values are $c_0 = 0.25$, $\tau_0 = 1$, $n = 1$, $a = 0.25$, while b and γ are given in the legends. Limit-cycle crossing rates: (c) $k(\tau)$ (see text) for the nonlinear system of Eq. (12) with $\mu = 1$, $\omega_0 = 1$, and noise parameters $c_0 = 0.05$, $\tau_0 = 1$, and $n = 1$. Vertical dashed lines represent the predicted resonance value of Eq. (4).

be calculated only analytically [30]. However, the numerical curves for $k(\tau)$ in Fig. 3(c) clearly exhibit autonomous SR for $\tau \simeq \tau_c$. Once again, the resonant dynamics is triggered by the optimal growth of σ^2_{qq} at the fixed point [compare with the curves in Fig. 3(c)], as energy is being pumped in from the fluctuating environment.

Before leaving this subsection we note that an approximate barrier crossing rate can be calculated for the present problem in the following way. The easy escape path occurs when both the recovering and the nonlinear damping force are vanishingly small, namely, for $q \simeq 0$ and $\dot{q} \simeq \pm 1/\mu$. An example of escape trajectory is shown in Fig. 4 for $\mu = 1$; under this circumstance, the particle most likely escapes the stable attractor through either phase-space point (0,1) or (0, −1). As mentioned above, the corresponding activation energy is $E_a \simeq \dot{q}^2/2$, the Boltzmann factor for either escape state being $e^{-\frac{E_a}{\langle \dot{q}^2 \rangle}}$. On assuming that the crossing attack rate coincides with the frequency of the damped oscillations in the basin of the stable attractor, one can approximate the escape rate, $k(\tau)$, as

$$k(\tau) = \frac{\omega_d}{2\pi} e^{-\frac{E_a}{\langle \dot{q}^2 \rangle}}. \tag{13}$$

Here ω_d and $\langle \dot{q}^2 \rangle$ are the angular frequency and the mean square velocity of the particle's damped oscillations given respectively in Eqs. (A5) and (B2) in the Appendices. Moreover, we have defined the escape time, $\tau_{\rm esc}$, as the time required by the particle placed at the origin (0,0) of its phase space to reach either escape point for the first time, hence $k = 2/\langle \tau_{\rm esc} \rangle$. To check the validity of our calculations we have compared the analytical results with the numerical data in Fig. 5. One may notice that Eq. (13) appears to underestimate the numerical data: this is a consequence of the nonlinear nature of the damping force, which would require a more refined analytical

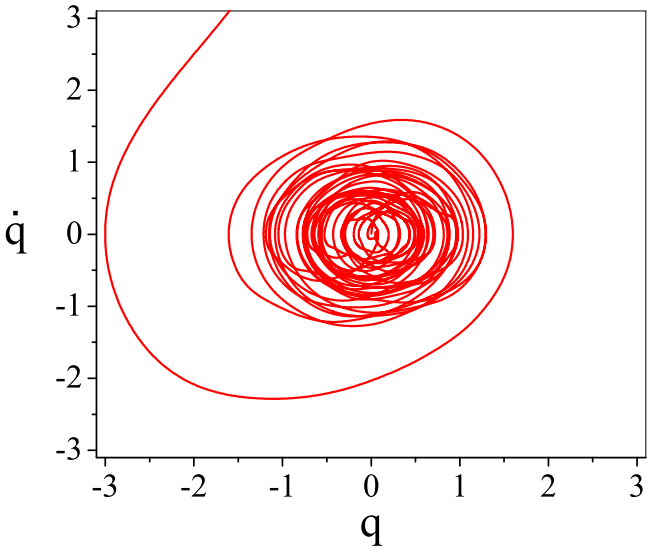

FIG. 4. Example of trajectory escaping through the unstable limit cycle of Eq. (8). The simulation parameter are $c_0 = 0.05$, $\tau = \tau_0 = n = 1$, $\gamma = 0.1$, $\mu = \omega_0 = 1$.

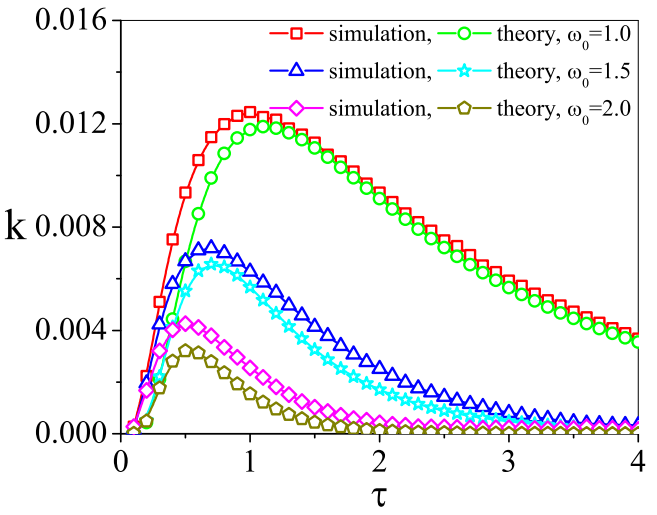

FIG. 5. Rate of escape $k(\tau)$ through the unstable limit cycle of Eq. (8) for $c_0 = 0.05$, $\tau_0 = n = 1$, $\gamma = 0.1$, $\mu = 1$, and different ω_0, theory vs simulation.

treatment. However, the locations of the $k(\tau)$ maxima are well predicted by the resonance condition of Eq. (4).

IV. CONCLUSION

While we restricted our analysis mostly to analytically manageable linear oscillators, autonomous SR is detectable in a wide category of nonlinear devices coupled to a generic time-correlated heat bath, including the nonlinear MEMS of Ref. [18]. For an underdamped system, the transfer function exhibits one or more peaks of finite width in correspondence with its dynamic resonance frequencies; as the noise's relaxation rate (i.e., the reciprocal of its correlation time) happens to fall within one such resonance peak, the ensuing energy flow from the bath to the system will enhance the device's response. In this regard we expect that autonomous SR is a common occurrence in many areas of natural sciences.

ACKNOWLEDGMENTS

B.C.B. is thankful to Prof. D. S. Ray for valuable discussions. S.M. and J.D. are thankful to the Government of India for financial support through CSIR and UGC, respectively.

APPENDIX A: SOLUTION OF THE LANGEVIN EQ. (1)

Our starting LE, Eq. (1), for the harmonic oscillator is linear and therefore analytically integrable. Its solution for $q(t)$ is

$$q(t) = q(0)\chi_q(t) + \dot{q}(0)\chi(t) + \int_0^t \chi(t')\eta(t')\,dt', \tag{A1}$$

where

$$\chi_q(t) = 1 - \omega_0^2 \int_0^t \chi(t')\,dt', \tag{A2}$$

and $\chi(t)$ in the Laplace inverse of

$$\tilde{\chi}(s) = \frac{1}{s^2 + s\gamma + \omega_0^2}, \tag{A3}$$

namely,

$$\chi(t) = \frac{1}{\omega_d}\sin(\omega_d t)\exp\left(-\frac{\gamma t}{2}\right), \tag{A4}$$

with

$$\omega_d = \sqrt{-\frac{\gamma^2}{4} + \omega_0^2}. \tag{A5}$$

On making use of Eq. (A1), the variance of $q(t)$ follows suit,

$$\begin{aligned}\sigma_{qq}^2 &= \langle [q(t) - \langle q(t)\rangle]^2\rangle \\ &= \int_0^t \chi(t-t_1)\,dt_1 \int_0^t \chi(t-t_2)\langle \eta(t_1)\eta(t_2)\rangle\,dt_2 \\ &= \frac{D}{\tau\omega^2}\left[\left(-\frac{C}{A} + \frac{F}{B}\right)I_1 + \left(-\frac{\omega^2}{A^2}C + \frac{\omega_0'}{B^2}F\right)I_2\right] + \frac{D}{\tau\omega^2}\left[\frac{\omega^2}{A^2}CFI_3 - \frac{1}{B}CFI_4 - \frac{\omega}{B^2}CFI_5\right],\end{aligned} \tag{A6}$$

where

$$I_1 = \frac{\gamma^2}{\gamma^2 + 4\omega_d^2}\left[-\frac{4\omega_0^2}{2\gamma^3}\exp(-\gamma t) + \frac{1}{2\gamma}\exp(-\gamma t)\cos(2\omega_d t) + \frac{2\omega_d^2}{\gamma^3} + \frac{\omega_d}{\gamma^2}\exp(-\gamma t)\sin(2\omega_d t)\right],$$

$$I_2 = \frac{\gamma^2}{\gamma^2 + 4\omega_d^2}\left[-\frac{1}{2\gamma}\sin(2\omega_d t)\exp(-\gamma t) - \frac{\omega_d}{\gamma^2}\cos(2\omega_d t)\exp(-\gamma t) + \frac{\omega_d}{\gamma^2}\right],$$

$$I_3 = \left[\frac{\omega_d}{B^2} - \frac{1}{B}\sin(\omega_d t)\exp(-Bt) - \frac{\omega_d}{B^2}\cos^2(\omega_d t)\exp(-Bt)\right],$$

$$I_4 = \left[\frac{\omega_d}{A^2}\sin(\omega_d t)\exp(-Bt) - \frac{1}{A}\sin^2(\omega_d t)\exp(-\gamma t) - \frac{\omega_d}{A^2}\sin(\omega_d t)\cos(\omega_d t)\exp(-\gamma t)\right],$$

and

$$I_5 = \left[\frac{\omega_d}{A^2}\cos(\omega_d t)\exp(-Bt) - \frac{1}{A}\cos(\omega_d t)\sin(\omega_d t)\exp(-\gamma t) - \frac{\omega_d}{A^2}\cos^2(\omega_d t)\exp(-\gamma t)\right]$$

are functions of time and $A = \gamma/2 - 1/\tau$, $B = \gamma/2 + 1/\tau$, $C = A^2/(A^2 + \omega_d^2)$, and $F = B^2/B^2 + \omega_d^2)$ are constants.

For asymptotically large times, σ_{qq}^2 approaches the stationary value

$$\sigma_{qq}^2 = \langle q^2\rangle = \frac{D}{\tau\omega_d^2}\left\{\left[\left(-\frac{C}{A} + \frac{F}{B}\right)\frac{2\omega_d^2}{\gamma^3}G\right] + \left[\frac{\omega_d}{\gamma^2}\left(-\frac{\omega_d^2}{A^2}C + \frac{\omega_d}{B^2}F\right)G + \frac{\omega_d^2}{A^2}\left(\frac{\omega_d^2}{B^2}\right)CF\right]\right\}, \tag{A7}$$

with

$$G = \frac{\gamma^2}{\gamma^2 + 4\omega_d^2}. \tag{A8}$$

APPENDIX B: RATE OF BARRIER CROSSING THROUGH A SADDLE POINT

The barrier crossing rate can be calculated by adopting the classic Kramers' technique (see references in the main text). To this purpose, we need the steady-state distribution functions at both the bottom of the wells and the top of the barrier of the bistable potential $U(q)$. Following Ref. [21], the Fokker-Planck (FP) equation around the well bottoms can be approximated to

$$\frac{\partial \rho(q,v,t)}{\partial t} = \left[-v\frac{\partial}{\partial q} + \omega_{\pm}^2 q\frac{\partial}{\partial v} + \gamma\frac{\partial v}{\partial v} + \phi(t)\frac{\partial^2}{\partial v^2} + \psi(t)\frac{\partial^2}{\partial q\,\partial v}\right]\rho(q,v,t), \tag{B1}$$

where $\omega_{\pm}$, $\phi(t)$ and $\psi(t)$ have been defined in the main text. All variances and cross-correlations appearing in $\phi(t)$ and $\psi(t)$ can be easily calculated from Eq. (1) by substituting ω_0 with $\omega_{\pm}$. The stationary variance for $q(t)$ is reported in Eq. (A7). In the same way, explicit asymptotic expressions can be readily obtained for the other two (cross)variances, as well:

$$\begin{aligned}
\sigma_{\dot q\dot q}^2 = {} & \frac{D}{\tau}\left[\frac{C}{AB}\left(1-\frac{\gamma}{2A}\right)+\frac{CG}{A\gamma}\left(\frac{\gamma}{2A}-1\right)\left(\frac{2\omega_d^2}{\gamma^2}+1\right)\right] \\
& +\frac{D}{\tau}\left[\frac{CG}{2A\gamma}\left(1+\frac{2\omega_d^2}{A\gamma}\right)+\frac{FG}{B\gamma}\left(1-\frac{\gamma}{2B}\right)\left(\frac{2\omega_d^2}{\gamma^2}+1\right)\right] \\
& -\frac{D}{\tau}\left[\frac{FG}{2B\gamma}\left(1+\frac{2\omega_d^2}{B\gamma}\right)-\frac{F\gamma}{2AB^2}\left(1-\frac{\gamma}{2A}\right)\right] \\
& -\frac{D}{\tau}\left\{\frac{\gamma}{2\omega_d}\left[\frac{CG\omega_d}{\gamma^2 A}\left(\frac{\gamma}{2A}-1\right)+\frac{CG\omega_d}{A^2\gamma}\left(1+\frac{\gamma A}{2\omega_d^2}\right)\left(\frac{2\omega_d^2}{\gamma^2}+1\right)\right]\right\} \\
& -\frac{D}{\tau}\left\{\frac{\gamma}{2\omega_d}\left[\frac{FG\omega_d}{\gamma^2 B}\left(1-\frac{\gamma}{2B}\right)+\frac{FG}{B^2\gamma}\left(1+\frac{\gamma B}{2\omega_d^2}\right)\left(\frac{2\omega_d^2}{\gamma^2}+1\right)\right]\right\}
\end{aligned} \tag{B2}$$

and

$$\begin{aligned}
\sigma_{q\dot q}^2 = {} & \frac{D}{\tau\omega_d}\left[\frac{CF\omega_d}{AB^2}\left(1-\frac{\gamma}{2A}\right)+\frac{G\omega_d}{\gamma^2 A}\left(\frac{\gamma}{2A}-1\right)+\frac{2G\omega_d^3}{\gamma^3 A^2}\left(1+\frac{\gamma A}{2\omega_d}\right)\right] \\
& +\frac{D}{\tau\omega_d}\left[\frac{FG\omega_d}{\gamma^2 B}\left(1-\frac{\gamma}{2B}\right)+\frac{C\omega_d}{A^2 B}\left(\frac{\gamma}{2B}-1\right)\right] \\
& +\frac{D}{\tau\omega_d}\left[\frac{FC\omega_d^2}{A^2B^2}\left(1+\frac{\gamma B}{2\omega_d^2}\right)-\frac{2G\omega_d^3}{\gamma^3 B^2}\left(1+\frac{\gamma B}{2\omega_d^2}\right)\right],
\end{aligned} \tag{B3}$$

where the constants A, B, C, F, and G are the same as in Appendix A upon replacing ω_0 with $\omega_{\pm}$.

Similarly, we wrote the FP equation for the particle dynamics around the barrier top (assuming the same diffusion coefficient), and following Kramers' Ansatz [22] we finally calculated the barrier crossing rate reported in the text.

[1] L. Gammaitoni, P. Hänggi, P. Jung, and F. Marchesoni, Stochastic resonance, Rev. Mod. Phys. **70**, 223 (1998); Stochastic resonance: A remarkable idea that changed our perception of noise, Eur. Phys. J. B **69**, 1 (2009).

[2] R. Benzi, Stochastic resonance: From climate to biology, Nonlin. Processes Geophys. **17**, 431 (2010).

[3] P. Hänggi, Stochastic resonance in biology, Chem. Phys. Chem. **3**, 285 (2002).

[4] V. S. Anishchenko, A. B. Neiman, F. Moss, and L. Schimansky-Geier, Stochastic resonance: Noise-enhanced order, Phys. Usp. **42**, 7 (1999).

[5] T. Wellens, V. Shatokhin, and A. Buchleitner, Stochastic resonance, Rep. Prog. Phys. **67**, 45 (2004).

[6] C. Presilla, F. Marchesoni, and L. Gammaitoni, Periodically time-modulated bistable systems: Nonstationary statitical properties, Phys. Rev. A **40**, 2105 (1989).

[7] P. Hänggi, P. Jung, C. Zerbe, and F. Moss, Can colored noise improve stochastic resonance? J. Stat. Phys. **70**, 25 (1993).

[8] Hu Gang, T. Ditzinger, C. Z. Ning, and H. Haken, Stochastic Resonance without External Periodic Force, Phys. Rev. Lett. **71**, 807 (1993).

[9] A. S. Pikovsky and J. Kurths, Coherence Resonance in a Noise-Driven Excitable System, Phys. Rev. Lett. **78**, 775 (1997).

[10] A. Longtin, Autonomous stochastic resonance in bursting neurons, Phys. Rev. E **55**, 868 (1997).

[11] P. S. Burada, G. Schmid, D. Reguera, M. H. Vainstein, J. M. Rubi, and P. Hänggi, Entropic Stochastic Resonance, Phys. Rev. Lett. **101**, 130602 (2008).

[12] P. K. Ghosh, F. Marchesoni, S. E. Savel'ev, and F. Nori, Geometric Stochastic Resonance, Phys. Rev. Lett. **104**, 020601 (2010).

[13] R. F. Fox and Yan-nan Lu, Analytic and numerical study of stochastic resonance, Phys. Rev. E **48**, 3390 (1993).

[14] M. Gitterman, Harmonic oscillator with multiplicative noise: Nonmonotonic dependence on the strength and the rate of dichotomous noise, Phys. Rev. E **67**, 057103 (2003).

[15] A. Fuliński, Relaxation, noise-induced transitions, and stochastic resonance driven by non-Markovian dichotomic noise, Phys. Rev. E **52**, 4523 (1995).

[16] L. Gammaitoni, F. Marchesoni, E. Menichella-Saetta, and S. Santucci, Multiplicative stochastic resonance, Phys. Rev. E. **49**, 4878 (1994).

[17] By means of a standard Mil'shtein algorithm, see P. E. Kloeden and E. Platen, *Numerical Solution of Stochastic Differential Equations* (Springer, Berlin, 1992).

[18] F. Cottone, H. Vocca, and L. Gammaitoni, Nonlinear Energy Harvesting, Phys. Rev. Lett. **102**, 080601 (2009).

[19] V. Méndez, D. Campos, and W. Horsthemke, Efficiency of harvesting energy from colored noise by linear oscillators, Phys. Rev. E **88**, 022124 (2013).

[20] P. Hänggi, P. Talkner, and M. Borkovec, Reaction rate theory: Fifty years after Kramers, Rev. Mod. Phys. **62**, 251 (1990).

[21] J. Das, S. Mondal, and B. C. Bag, Fokker-Planck equation for the non-Markovian Brownian motion in the presence of a magnetic field, J. Chem. Phys. **147**, 164102 (2017).

[22] S. K. Banik, J. R. Chaudhuri, and D. S. Ray, The generalized Kramers theory for nonequilibrium open one-dimensional systems, J. Chem. Phys. **112**, 8330 (2000).

[23] P. Hänggi, F. Marchesoni, and P. Grigolini, Bistable flow driven by coloured Gaussian noise: A critical study, Z. Phys. B **56**, 333 (1984).

[24] F. Marchesoni, E. Menichella-Saetta, M. Pochini, and S. Santucci, Analog simulation of underdamped stochastic systems driven by colored noise: Spectral densities, Phys. Rev. A **37**, 3058 (1988).

[25] C. R. Doering and J. C. Gadoua, Resonant Activation over a Fluctuating Barrier, Phys. Rev. Lett. **69**, 2318 (1992).

[26] M. Marchi, F. Marchesoni, L. Gammaitoni, E. Menichella-Saetta, and S. Santucci, Resonant activation in a bistable system, Phys. Rev. E **54**, 3479 (1996).

[27] See, e.g., Van der Pol equation, in *Encyclopedia of Mathematics*, ed. M. Hazewinkel (Kluwer, Dordrecht, 2001).

[28] M. K. Sen, A. Baura, and B. C. Bag, Noise induced escape through an unstable limit cycle in the presence of a fluctuating barrier, J. Stat. Mech. (2009) P11004.

[29] V. I. Nekorkin and V. A. Makarov, Spatial Chaos in a Chain of Coupled Bistable Oscillators, Phys. Rev. Lett. **74**, 4819 (1995); V. Krivan and J. Eisner, Optimal foraging and predator-prey dynamics, Theor. Popul. Biol. **63**, 269 (2003); P. Ghosh, S. Sen, S. S. Riaz, and D. S. Ray, Controlling birhythmicity in a self-sustained oscillator by time-delayed feedback, Phys. Rev. E **83**, 036205 (2011).

[30] R. S. Maier and D. L. Stein, Oscillatory Behavior of the Rate of Escape Through an Unstable Limit Cycle, Phys. Rev. Lett. **77**, 4860 (1996).